International Journal of Control
Publication details, including instructions for authors and subscription information:
http://www.tandfonline.com/loi/tcon20

Parameter identification of aggregated thermostatically controlled loads for smart grids using PDE techniques

Scott Moura[a], Jan Bendtsen[b] & Victor Ruiz[c]

[a] Department of Civil and Environmental Engineering, University of California Berkeley, Berkeley, CA 94720, USA

[b] Department of Electronic Systems, Automation and Control, Aalborg University, Fr. Bajers Vej 7C, 9220 Aalborg, Denmark

[c] Department of Mechanical and Aerospace Engineering, University of California San Diego, 9500 Gilman Drive, La Jolla, CA 92093, USA

Accepted author version posted online: 14 Apr 2014.Published online: 06 May 2014.

To cite this article: Scott Moura, Jan Bendtsen & Victor Ruiz (2014) Parameter identification of aggregated thermostatically controlled loads for smart grids using PDE techniques, International Journal of Control, 87:7, 1373-1386, DOI: 10.1080/00207179.2014.915083

To link to this article: http://dx.doi.org/10.1080/00207179.2014.915083

International Journal of Control, 2014
Vol. 87, No. 7, 1373–1386, http://dx.doi.org/10.1080/00207179.2014.915083

Parameter identification of aggregated thermostatically controlled loads for smart grids using PDE techniques

Scott Moura[a,*], Jan Bendtsen[b] and Victor Ruiz[c]

[a]*Department of Civil and Environmental Engineering, University of California Berkeley, Berkeley, CA 94720, USA;* [b]*Department of Electronic Systems, Automation and Control, Aalborg University, Fr. Bajers Vej 7C, 9220 Aalborg, Denmark;* [c]*Department of Mechanical and Aerospace Engineering, University of California San Diego, 9500 Gilman Drive, La Jolla, CA 92093, USA*

(*Received 11 March 2013; accepted 26 February 2014*)

This paper develops methods for model identification of aggregated thermostatically controlled loads (TCLs) in smart grids, via partial differential equation (PDE) techniques. Control of aggregated TCLs provides a promising opportunity to mitigate the mismatch between power generation and demand, thus enhancing grid reliability and enabling renewable energy penetration. To this end, this paper focuses on developing parameter identification algorithms for a PDE-based model of aggregated TCLs. First, a two-state boundary-coupled hyperbolic PDE model for homogenous TCL populations is derived. This model is extended to heterogeneous populations by including a diffusive term, which provides an elegant control-oriented model. Next, a passive parameter identification scheme and a swapping-based identification scheme are derived for the PDE model structure. Simulation results demonstrate the efficacy of each method under various autonomous and non-autonomous scenarios. The proposed models can subsequently be employed to provide system critical information for power system monitoring and control.

Keywords: distributed parameter systems; model identification; smart grids; parameter estimation; demand side management

1. Introduction

One of the main challenges in achieving significant penetration of renewables in future power systems is their inherent variability (see e.g. Banakar, Luo, & Ooi, 2008). In recent years, *demand side management* has gained attention as a means to balance power supply and demand, in the presence of intermittent power sources (Mohsenian-Rad, Wong, Jatskevich, Schober, & Leon-Garcia, 2010; Short, Infield, & Freris, 2007; Strbac, 2008; Walawalkar, Blumsack, Apt, & Fernands, 2008). In spite of growing overall consumption and increased penetration of renewables, new investments on the demand side may have greater impact than on the supply side (International Energy Agency, 2006). In particular, the intermittency and non-dispatchability associated with renewable energy sources can be partially mitigated by flexible loads. Conventional generation, the alternative option, typically exhibits longer response time and can be an expensive and environmentally damaging method for mitigating fluctuations in renewable generation (Klobasa, 2010; Strbac, 2008).

Various technologies are being considered for demand side management. Examples include coordinated charging of electric vehicle batteries (Mets, Verschueren, Haerick, Develder, & Turck, 2010), deliberate scheduling of loads with flexible deadlines (Petersen, Bendtsen, & Stoustrup, 2012), or allowing local consumers with slow dynamics (large time constants) to adjust their consumption (see e.g. Moslehi & Kumar, 2010). A particularly promising method is to exploit the large thermal time constants in so-called *thermostatically controlled loads* (TCLs), such as deep freezers, refrigerators, local heat pumps, etc. Some heating, ventilation, and air conditioning systems (HVAC) in town houses, cooling systems in storage buildings, etc. also fall into this category. TCLs operate in cycles by switching between 'ON' (drawing electrical power) and 'OFF' (not drawing any power). The devices have been thoroughly studied, and models of varying complexity are readily available. Various methods have been studied to derive population models from individual TCL models, such as aggregation (Bompard, Carpaneto, Chicco, & Napoli, 1996), clustering (Zhang, Lian, Chang, Kalsi, & Sun, 2012), and state queueing (Lu, Chassin, & Widergren, 2005).

An entity – for example, a utility company – interested in direct load control of TCLs for power demand/supply balancing may take different approaches to regulating aggregate power consumption. However, to directly manipulate the individual units' power consumption, the utility control system in principle requires knowledge of all system states, as well as control authority over individual power consumption. Thus, controlling individual units typically

* Corresponding author. Email: smoura@berkeley.edu

require detailed local measurement and feedback of current energy and power demands (McDonald, 2008), but has been shown to be feasible in practice for limited numbers of units (Andersen, Pedersen, & Nielsen, 2012).

For large load populations, scalability is a key issue. In particular, attempting to control each individual unit directly leads to a heavy communication and computational burden on the system. Thus, rather than attempting to control every consumer individually, methods for modelling, estimating, and eventually controlling the behaviour of large populations of consumers have come into focus in recent years (Callaway, 2009; Callaway & Hiskens, 2011; Malhame & Chong, 1985; Mathieu, Koch, & Callaway, 2013). In this paradigm, one manipulates the operating conditions of the entire population. Example of control signals include temperature set-point deviations, temperature deadband size, and forced switching. The goal is to manipulate total power consumption while imposing minimal discomfort to the consumers. The most common approach in the literature models these large TCL populations via probability distributions and applies set-point control (Bashash & Fathy, 2013; Callaway, 2009; Kundu & Sinitsyn, 2012; Perfumo, Kofman, Braslavsky, & Ward, 2012).

This paper focuses on modelling and parameter identification of aggregated TCLs, to facilitate control schemes. In particular, we examine the dynamic behaviour of the temperature distribution in large TCL populations. The temperature distribution models available energy storage and, hence, the range in which the temperature set points can be manipulated to shape power flow. Given an accurate temperature distribution, the TCL population can be utilised as a 'virtual power plant' that provides services to the grid, such as frequency control and peak shaving.

We consider a large population of TCLs and derive two partial differential equation (PDE) based models for the temperature distribution evolution. The first model assumes that all loads are identical, and has been similarly derived by Malhame and Chong (1985) from a probabilistic viewpoint. We propose a new model to account for parameter heterogeneity, by including a diffusion term in the boundary-coupled PDE model. In doing so, we expand upon existing PDE-based TCL models (Bashash & Fathy, 2013), which do not take inhomogeneity explicitly into account. The transfer function model of Perfumo et al. (2012) predicts the aggregate power response to step changes in temperature set points. In contrast, the PDE models are (infinite-dimensional) state-space models. That is, they capture the spatio-temporal dynamics of the population's temperature distribution. Both models are amenable to regulating aggregate power. However, the PDE models are also amenable to state observer designs (Moura, Ruiz, & Bendsten, 2013), which is a criterion for our model development. Next, we proposed two parameter estimation algorithms to identify the proposed PDE model in real time. The two algorithms include a passive and a swapping approach. In both cases, the algorithms utilise full-state measurements. We derive the signal properties of each identification scheme, and explore their behaviour under non-ideal scenarios via simulation examples. The simulations demonstrate how the algorithms can estimate the PDE model parameters in real time, given measurements from a population of individual stochastic TCLs, in both autonomous and controlled situations. As such, the proposed model and model identification algorithms can be used to monitor large aggregations of controllable flexible loads for demand side management services.

The remainder of the paper is outlined as follows. Section 2 presents a hybrid ordinary differential equation (ODE) model of a single TCL. Section 3 presents two PDE models of TCL populations, corresponding to homogeneous and heterogeneous populations. Sections 4.1 and 4.2 present a passive and a swapping-based continuous-time parameter identification scheme, respectively. Signal properties for each method are derived via Lyapunov techniques. Section 5 examines each identification scheme under non-ideal scenarios via simulation, and compares these methods. Finally, Section 6 offers concluding remarks and future work.

2. Thermostatically controlled loads

This section presents a simple TCL model, which serves as the basis for subsequent population models.

Denote the thermal zone and ambient temperatures for the ith load by $T_i(t)$ and $T_{\infty,i}(t)$, respectively. Note that the ambient temperature can be time-varying. Assume that the hardware is purely on/off regulated. For simplification of presentation, we shall assume a population containing cooling loads only. The generalisation to mixed cooling/heating loads requires minor adjustments to the mathematical structure. Then we can derive the following simple hybrid ODE model (Callaway, 2009; Malhame & Chong, 1985; Perfumo et al., 2012):

$$\dot{T}_i(t) = \frac{1}{R_i C_i}[T_{\infty,i}(t) - T_i(t) - s_i(t) R_i P_i + w(t)], \quad i = 1, 2, \ldots, N \tag{1}$$

$$s_i(t) = \begin{cases} 0 & \text{if } s_i(t-\varepsilon) = 1 \text{ and } T_i(t) \le T_{\min,i} \\ 1 & \text{if } s_i(t-\varepsilon) = 0 \text{ and } T_i(t) \ge T_{\max,i} \\ s_i(t-\varepsilon) & \text{otherwise} \end{cases} \tag{2}$$

for some small time ε. The symbol $C_i \in \mathbb{R}_+$ is the thermal capacitance (kWh/°C), $R_i \in \mathbb{R}_+$ is the corresponding thermal resistance (°C/kW), and $P_i \in \mathbb{R}$ is the (constant) cooling power supplied by the hardware when switched on. Variable $s_i \in \{0, 1\}$ is a Boolean-valued quantity that determines the hardware's on/off state. It switches status whenever the internal temperature encounters the limits of a

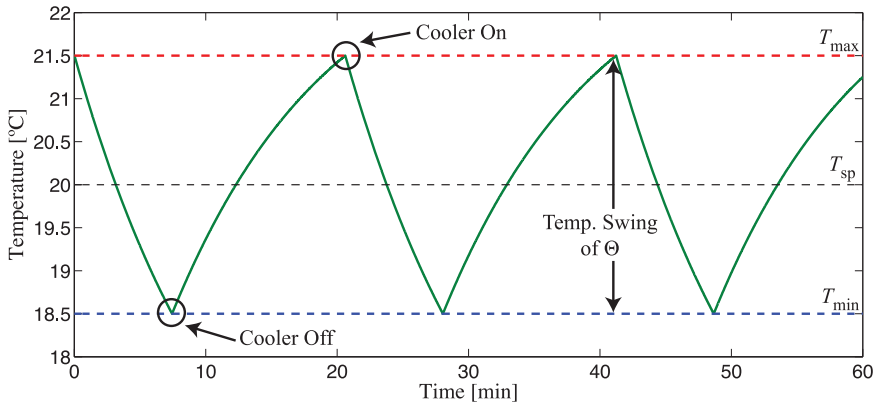

Figure 1. Evolution of temperature for a typical thermostatically controlled load.

preset temperature span $[T_{\min,i}, T_{\max,i}] \subset \mathbb{R}$. The term $w(t)$ encapsulates thermal disturbances due to occupancy, open windows/doors, etc. The general behaviour is demonstrated graphically in Figure 1.

Note that the dynamical structure is identical for heating and cooling systems. Whether the device operates as a heating or cooling system is only a matter of whether T_∞ is higher or lower than the operating interval, as well as the sign of $s_i(t)R_iP_i$. In Figure 1, we have $T_\infty > T_{\max}$ and $s(t)RP \geq 0$ for $t \geq 0$.

The temperature limits $T_{\min,i}$ and $T_{\max,i}$ are related to the ith load's *set point* $T_{\text{sp},i}$ through the following fixed relations:

$$T_{\min,i} = T_{\text{sp},i} - \frac{\Theta_i}{2}, \quad T_{\max,i} = T_{\text{sp},i} + \frac{\Theta_i}{2}$$

where Θ_i is the width of the temperature interval. Furthermore, the cumulative power consumption of the population of TCLs at any given time t can be computed as

$$P(t) = \sum_{i=1}^{N} \frac{P_i s_i(t)}{\eta_i} \tag{3}$$

where η_i is the coefficient of performance for the ith heating/cooling unit.

2.1 *Simulations*

Figure 2 demonstrates the aggregated behaviour for 25 identical TCLs. The left plots show how the TCLs alternate between the *on* and *off* states while remaining within the operation band. The TCLs were initialised at random temperatures, with a quartic distribution around 20 °C, all in the *off* state, with parameters adopted from Callaway (2009) and Perfumo et al. (2012) and given in Table 1. As can be seen, the power drawn by the population oscillates with a constant amplitude, since the TCLs are synchronised.

The right plots show a similar situation, however, the TCL time constants are now drawn from a random distribution, thus making the population *heterogenous*. The corresponding power trace exhibits a damped oscillation. Namely, it oscillates to start, but due to different time constants the individual TCLs gradually de-synchronise and the oscillations damp out. Damped oscillations similarly occur if other parameters, such as Θ_i or $T_{\infty,i}$, are allowed to vary across the TCL population.

As the number of units grow, the computational load required to simulate the individual TCLs (referred to as *Monte Carlo* (MC) simulations) grows significantly and eventually becomes intractable. Instead, the characteristic behaviours outlined above will be captured in partial differential models that describe how the distribution of temperature in the population evolves across the temperature range.

3. Aggregate TCL modelling via PDEs

Consider a large population of TCLs evolving over a finite temperature interval $[\underline{T}, \overline{T}]$, which we assume to be known and constant. The TCLs in the *on* state gradually decrease until they reach $T_{\min,i}$, at which point they switch to the *off* state. Conversely, the TCLs in the *off* state gradually increase until they reach $T_{\max,i}$. This evolution can be modelled as a set of coupled PDEs with boundary conditions (Malhame & Chong, 1985). Previous studies by Malhame and Chong (1985), Callaway (2009), and Bashash and Fathy (2013) generate a probabilistic interpretation of these PDEs (i.e. Fokker–Plank equations) and define the states on an infinite domain. In contrast, we model the deterministic evolution on a finite-temperature domain. The derivation follows concepts from fluid mechanics. In contrast to Bashash and Fathy (2013), the following derivation does not assume constant transport speeds, thereby producing reaction terms in the PDEs. Moreover, we consider time-varying ambient temperature $T_\infty(t)$, thus producing time-varying transport speeds.

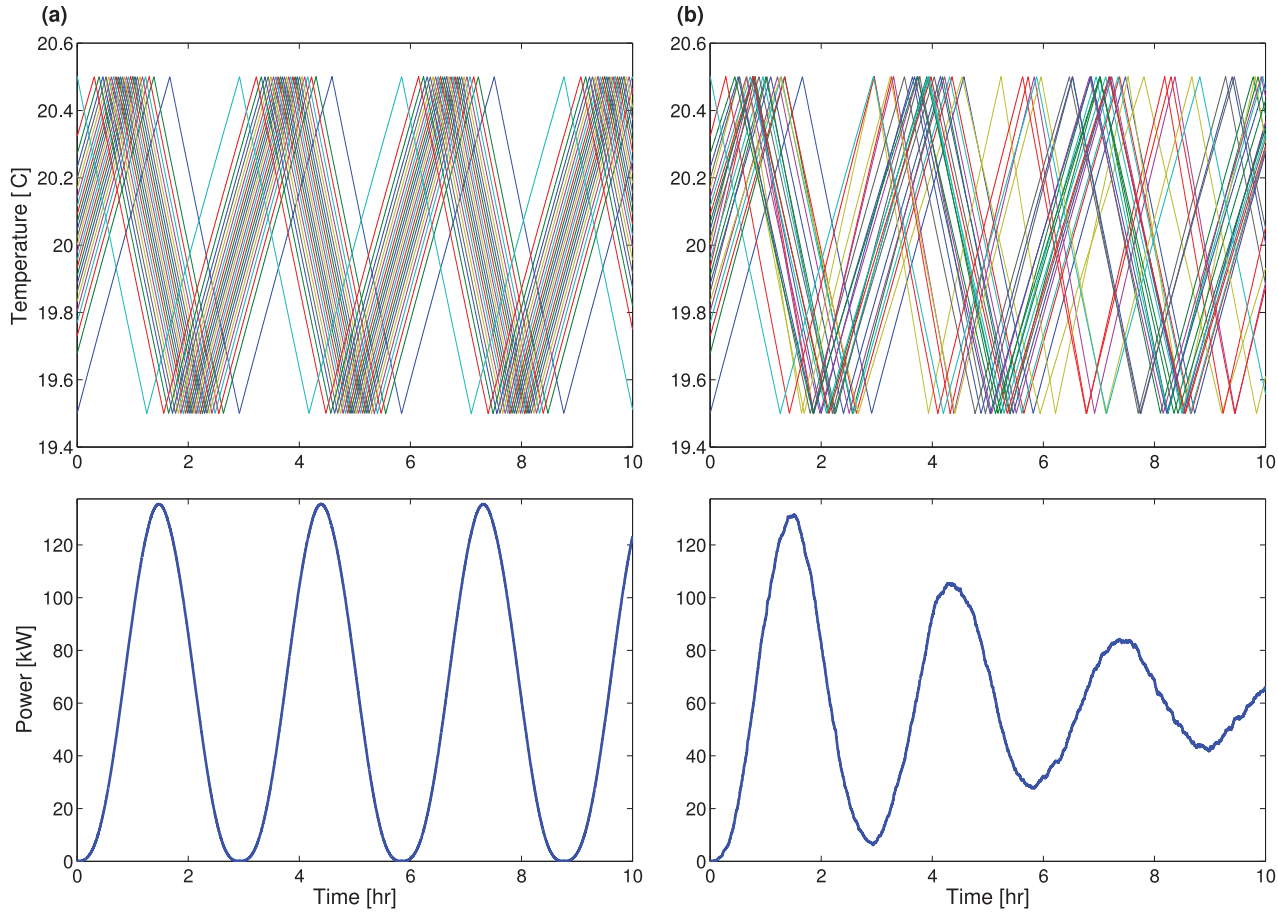

Figure 2. Evolution of temperature for 25 TCLs from (a) homogeneous and (b) heterogeneous populations. In each case, the population was initialised with all TCLs in the *off* state, with temperature distributed according to $u_0(T)$, $v_0(T)$ in Table 1. Note that the TCLs remain in synchrony for the homogenous population. In contrast, the temperature distribution diffuses in the heterogeneous case. This observation motivates the heterogeneous model in Section 3.2.

3.1 *PDE model for homogeneous populations*

Let the states $u(T, t)$ and $v(T, t)$, both defined on the space $[\underline{T}, \overline{T}] \times \mathbb{R}_+ \to \mathbb{R}$, denote the temperature distribution at temperature T and at time t in the *on* and *off* states, respectively. Henceforth, we assume a homogeneous population, where the parameters R_i, C_i, P_i, $T_{\min,i}$, and $T_{\max,i}$ are equal for all TCLs. Consequently, the 'flux' of TCLs that traverses temperature T at time t in either the increasing or the

Table 1. Homogeneous and heterogeneous model parameter values adopted from Callaway (2009) and Perfumo et al. (2012).

Parameter	Description [unit]	Homogeneous	Heterogeneous
R	Thermal resistance [°C/kW]	2	2
C	Thermal capacitance [kWh/°C]	10	$\sim\mathcal{N}(10, 1)$
P	Thermal power [kW]	14	14
T_∞	Ambient temperature [°C]	32	32
T_{sp}	Temperature set point [°C]	20	20
Θ	Temperature deadband width [°C]	1	1
η	Coefficient of performance [–]	2.5	2.5
β	Diffusivity [(°C)^3/s]	–	0.01
$u_0(T)$	Initial distribution of *on* TCLs [TCLs/°C]	0	0
$v_0(T)$	Initial distribution of *off* TCLs [TCLs/°C]	$\frac{30N}{16\Theta}\left[1-\frac{4}{\Theta^2}(T-T_{\text{sp}})^2\right]^2$	$\frac{30N}{16\Theta}\left[1-\frac{4}{\Theta^2}(T-T_{\text{sp}})^2\right]^2$
σ_w	Standard deviation of thermal disturbance in Equation (1)	0	0.01

decreasing direction can be written as

$$\phi(T,t) = u(T,t)\frac{dT}{dt}\bigg|_{s=1} \text{ and } \psi(T,t) = v(T,t)\frac{dT}{dt}\bigg|_{s=0} \tag{4}$$

respectively. Substituting Equation (1) and disregarding disturbance term $w(t)$ into the equations above we get

$$\phi(T,t) = \frac{1}{RC}(T_\infty(t) - T(t) - RP)u(T,t) \tag{5}$$

$$\psi(T,t) = \frac{1}{RC}(T_\infty(t) - T(t))v(T,t) \tag{6}$$

Next, let us consider the small control volume of width δT shown in Figure 3. Using standard limit arguments, we get the relation

$$\begin{aligned}\frac{\partial v}{\partial t}(T,t) &= \lim_{\delta T\to 0}\left[\frac{\psi(T+\delta T,t) - \psi(T,t)}{\delta T}\right] \\ &= \frac{\partial \psi}{\partial T}(T,t) \\ &= -\frac{1}{RC}\left[T_\infty(t) - T(t)\right]\frac{\partial v}{\partial T}(T,t) + \frac{1}{RC}v(T,t)\end{aligned} \tag{7}$$

for the TCLs in the *off* state and, correspondingly,

$$\begin{aligned}\frac{\partial u}{\partial t}(T,t) &= -\frac{\partial}{\partial T}\left[\frac{1}{RC}(T_\infty - T(t) - RP)u(T,t)\right] \\ &= -\frac{1}{RC}\left[T_\infty(t) - T(t) - RP\right]\frac{\partial u}{\partial T}(T,t) \\ &\quad + \frac{1}{RC}u(T,t)\end{aligned} \tag{8}$$

for the TCLs in the *on* state.

As the temperatures of TCLs in the *on* state reach $T_{\min}$, they switch to the *off* state, and vice versa at $T_{\max}$. This gives rise to coupling between the two PDEs indicated in Figure 3:

$$\phi(T_{\max}^+, t) + \phi(T_{\max}^-, t) + \psi(T_{\max}, t) = 0$$
$$\psi(T_{\min}^-, t) + \psi(T_{\min}^+, t) + \phi(T_{\min}, t) = 0$$

where $\phi(T_{\max}^+, t)$ is the flux of TCLs coming from higher temperatures than $T_{\max}$, $\phi(T_{\max}^-, t)$ is the flux of TCLs just inside the temperature band and $\psi(T_{\max}, t)$ is the number of units switching from the *off* state to the *on* state per time unit. $\psi(T_{\min}^-, t)$, $\psi(T_{\min}^+, t)$, and $\phi(T_{\min}, t)$ are defined analogously. Finally, we shall impose the condition that the flux tends to zero at the temperature extremes, i.e. $\phi(\overline{T}, t) = \psi(\underline{T}, t) = 0$.

After some time of operation, there will be no TCLs outside the interval $[T_{\min}, T_{\max}]$, in which case the coupling equations reduce to

$$\phi(T_{\max}^-, t) + \psi(T_{\max}, t) = 0 \tag{9}$$

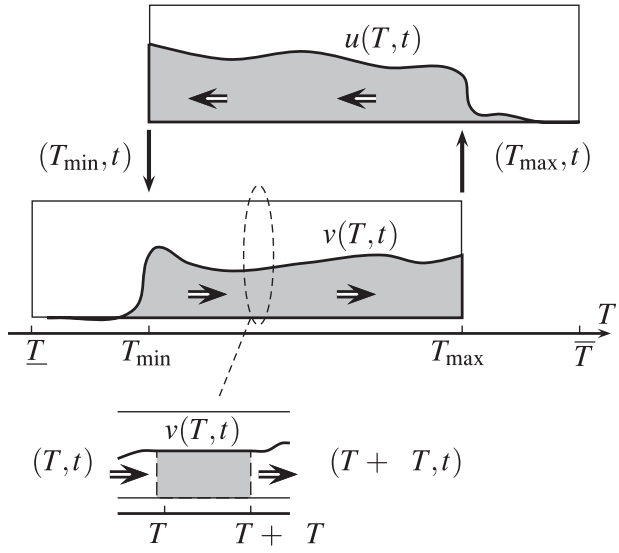

Figure 3. Illustration of transport PDE representation of temperature distributions; $u(T, t)$ is the *on* state distribution, while $v(T, t)$ is the *off* state distribution. The bottom part of the figure shows a zoom on a small control volume of width δT, in which $v(T, t)$ is assumed to be constant.

$$\psi(T_{\min}^+, t) + \phi(T_{\min}, t) = 0 \tag{10}$$

or

$$u(T_{\max}, t) = -\frac{T_\infty(t) - T_{\max}}{T_\infty(t) - T_{\max} - RP}v(T_{\max}, t)$$

$$v(T_{\min}, t) = -\frac{T_\infty(t) - T_{\min} - RP}{T_\infty(t) - T_{\min}}u(T_{\min}, t)$$

For compactness of notation, we write the homogeneous TCL PDE model as

$$u_t(T,t) = \alpha\lambda(T,t)u_T(T,t) + \alpha u(T,t) \tag{11}$$

$$v_t(T,t) = -\alpha\mu(T,t)v_T(T,t) + \alpha v(T,t) \tag{12}$$

$$u(T_{\max}, t) = q_1(t)v(T_{\max}, t) \tag{13}$$

$$v(T_{\min}, t) = q_2(t)u(T_{\min}, t) \tag{14}$$

where the parameters $\alpha, \lambda(T), \mu(T), q_1$, and q_2 are given by

$$\alpha = \frac{1}{RC} > 0 \tag{15}$$

$$\lambda(T,t) = -(T_\infty(t) - T - RP) > 0 \tag{16}$$

$$\mu(T,t) = T_\infty(t) - T > 0 \tag{17}$$

$$q_1(t) = -\frac{T_\infty(t) - T_{\max}}{T_\infty - T_{\max} - RP} \tag{18}$$

$$q_2(t) = -\frac{T_\infty(t) - T_{\min} - RP}{T_\infty - T_{\min}} \tag{19}$$

and the corresponding total power consumption is

$$P(t) = \frac{P}{\eta}\int_{T_{\min}}^{T_{\max}} u(T,t)dT$$

where η is the coefficient of performance for the TCLs.

Remark 1: Note that the homogeneous PDE model (11)–(14) satisfies the model property that the total number of TCLs is conserved over time. Although this property is trivially satisfied in the homogeneous case, it plays an important role in the following heterogeneous PDE derivation.

Note that the preceding PDE model derivation assumes a homogeneous population of TCLs. In practice, TCLs exhibit parameter heterogeneity. That is, the heat capacities, heating resistances, ambient temperatures, cooling power, temperature deadband sizes, etc. may vary. For this reason, we modify the model above to account for heterogeneous populations of TCLs in the following.

3.2 *PDE model for heterogeneous populations*

Motivated by the diffusive phenomenon observed in the MC simulations of heterogeneous populations, we consider the following PDE model:

$$u_t(T,t) = \alpha\lambda(T,t)u_T(T,t) + \alpha u(T,t) + \beta u_{TT}(T,t) \tag{20}$$

$$v_t(T,t) = -\alpha\mu(T,t)v_T(T,t) + \alpha v(T,t) + \beta v_{TT}(T,t) \tag{21}$$

$$u(T_{\max},t) = q_1(t)v(T_{\max},t) \tag{22}$$

$$v(T_{\min},t) = q_2(t)u(T_{\min},t) \tag{23}$$

$$u_T(T_{\min},t) = -v_T(T_{\min},t) \tag{24}$$

$$v_T(T_{\max},t) = -u_T(T_{\max},t) \tag{25}$$

This model adds diffusion terms to PDEs (11) and (12) to incorporate parameter heterogeneity, based upon observations of the heterogeneous MC simulations in Section 2.1. The two boundary conditions (24) and (25) are added to preserve well-posedness of the PDE system. In particular, these additional boundary conditions ensure that the total number of TCLs is conserved.

Lemma 3.1 (*Conservation of TCLs for heterogeneous model*): *Consider the coupled PDE system* (20)–(25) *for heterogeneous TCL populations. Define the quantity as follows:*

$$N(t) = \int_{T_{\min}}^{T_{\max}} u(T,t)dT + \int_{T_{\min}}^{T_{\max}} v(T,t)dT \tag{26}$$

which represents the total number of TCLs at a given time t. Then,

$$\frac{d}{dt}N(t) = 0, \qquad \forall t \in \mathbb{R} \tag{27}$$

Proof: The proof consists of three steps: (1) differentiate Equation (26) with respect to time along the trajectories of Equations (20) and (21), (2) apply integration by parts, and (3) utilise the boundary conditions (22)–(25). □

3.3 *Simulations*

Next, we study simulations of the homogeneous and heterogeneous PDE models. Parameter values and initial conditions for the models are adopted from Callaway (2009) and Perfumo et al. (2012), and given in Table 1. The homogeneous and heterogeneous models are implemented using the MacCormack (MacCormack, 2003) and Crank–Nicolson (Crank & Nicolson, 1947) finite-differencing methods, respectively. Both models are initialised with all TCLs in the *off* state, with a quartic distribution about the set-point temperature $T_{sp} = 20\ ^\circ$C. Note that any initial condition for the PDE model can be selected, provided it satisfies boundary conditions (22)–(25), and thus ensures well-posedness. For the heterogeneous PDE, $\alpha = 1/RC$ where C is the mean value from Table 1. Parameter β is selected via an offline optimisation routine which minimises the integrated square error between the MC and PDE simulations in Figure 5.

Figure 4 demonstrates how the PDE states evolve in temperature and time. For the homogeneous model, one can see that the distribution of TCLs migrates across the temperature deadband in an oscillatory fashion. Similarly, the heterogeneous model exhibits an oscillatory response, albeit with damping induced by the diffusion term. Figure 5 compares the aggregate power of 1000 individual TCLs (MC model) versus the PDE models, for both homogeneous and heterogeneous parameter sets. The homogeneous PDE model captures the dynamical effect of undamped oscillations. In addition, the heterogeneous PDE model captures the damped oscillations exhibited by 1000 individual TCL models. Furthermore, the PDE models reduce computation time by almost two orders of magnitude, as evidenced by the simulation times provided in Table 2. These simulations were performed on a laptop with a 2.7 GHz dual-core processor and 4 GB of RAM.

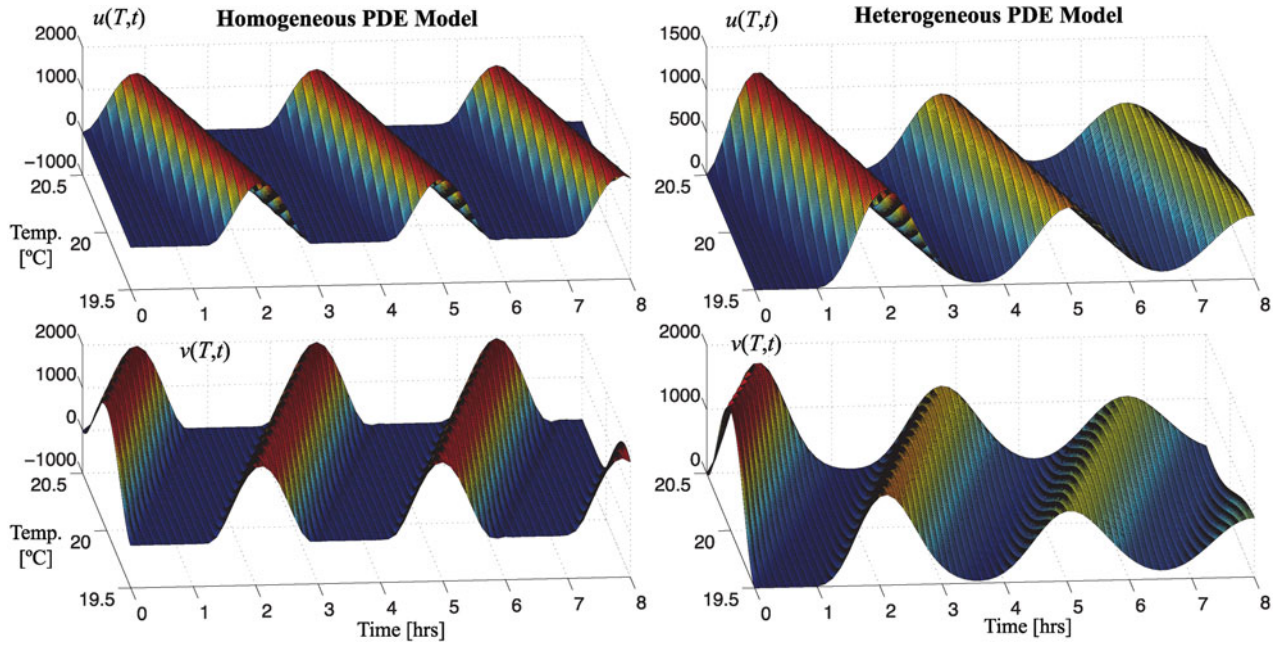

Figure 4. Evolution of temperature distributions for the homogeneous (left column) and heterogeneous (right column) PDE models. In the homogeneous model, the TCLs remain in synchrony. In the heterogeneous model, the TCL distribution diffuses due to parameter heterogeneity.

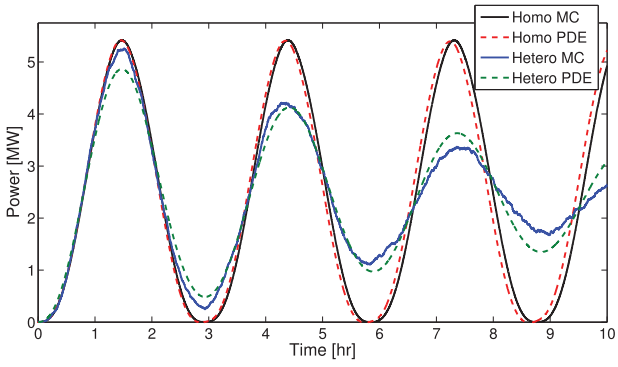

Figure 5. Comparison of aggregate TCL power for the homogeneous and heterogeneous populations, using the 1000 individual TCLs in the MC and the PDE models. The heterogeneous PDE model captures the damped oscillations exhibited by the 1000 individual TCL models.

4. Parameter identification

In this section, we provide the main contributions of this work, namely, two parameter identification schemes for the PDE model (20)–(25), and show that they are bounded in terms of error norms. Both methods assume full-state measurements of the temperature distribution. In practice, the distribution can be processed from sampled measurements of every TCL temperature in the population. That is, one can compute a histogram with respect to temperature, at each sampling instance.

As a preliminary step, we first normalise the temperature coordinate to simplify our analysis, by applying the linear transformation

$$x = \frac{T - T_{\min}}{T_{\max} - T_{\min}} \tag{28}$$

which renders the heterogenous PDE into

$$u_t(x,t) = \alpha\check{\lambda}(x,t)u_x(x,t) + \alpha u(x,t) + \check{\beta}u_{xx}(x,t) \tag{29}$$

$$v_t(x,t) = -\alpha\check{\mu}(x,t)v_x(x,t) + \alpha v(x,t) + \check{\beta}v_{xx}(x,t) \tag{30}$$

$$u(1,t) = q_1(t)v(1,t), \qquad u_x(0,t) = -v_x(0,t) \tag{31}$$

$$v(0,t) = q_2(t)u(0,t), \qquad v_x(1,t) = -u_x(1,t) \tag{32}$$

where the parameters $\check{\lambda}(x)$, $\check{\mu}(x)$, and $\check{\beta}$ are given by

$$\check{\lambda}(x,t) = x - \frac{T_\infty(t) - T_{\min} - RP}{T_{\max} - T_{\min}} \tag{33}$$

$$\check{\mu}(x,t) = \frac{T_\infty(t) - T_{\min}}{T_{\max} - T_{\min}} - x \tag{34}$$

Table 2. Comparison of simulation times for MC (individual) and PDE models.

	Homogeneous (s)	Heterogeneous (s)
Individual models	60.98	60.48
PDE model	1.08	1.86

$$\breve{\beta} = \frac{\beta}{(T_{\max} - T_{\min})^2} \tag{35}$$

To reduce notational clutter, the breves are henceforth dropped from $\breve{\lambda}(x,t)$, $\breve{\mu}(x,t)$, and $\breve{\beta}$.

Remark 2: In the following we assume constant ambient temperature T_∞. A straightforward extension of the proposed identifiers is to incorporate time-varying and measured T_∞, provided $T_\infty(t) > T_{\max}\ \forall\, t$. In this case, the algorithms contain time-varying terms $\lambda(x,t)$ and $\mu(x,t)$.

4.1 *Passive identifier*

Now, suppose the parameters α and β are uncertain, and exist on the domains $\alpha \geq \underline{\alpha} > 0$ and $\beta \geq \underline{\beta} > 0$. We seek to identify $\alpha, \beta \in \mathbb{R}$ in real time, from measurements of the states u, v. Inspired by Smyshlyaev and Krstic (2010), we introduce the following auxiliary system:

$$\hat{u}_t = \hat{\alpha}\lambda(x,t)\hat{u}_x + \hat{\beta}\hat{u}_{xx} + \hat{\alpha}u + \gamma^2(u-\hat{u})\|u\|^2 \tag{36}$$

$$\hat{v}_t = -\hat{\alpha}\mu(x,t)\hat{v}_x + \hat{\beta}\hat{v}_{xx} + \hat{\alpha}v + \gamma^2(v-\hat{v})\|v\|^2 \tag{37}$$

$$\hat{u}(1,t) = q_1(t)v(1,t), \qquad \hat{u}_x(0,t) = -v_x(0,t) \tag{38}$$

$$\hat{v}(0,t) = q_2(t)u(0,t), \qquad \hat{v}_x(1,t) = -u_x(1,t) \tag{39}$$

where $\hat{\alpha}$ and $\hat{\beta}$ are the parameter estimates, and $\gamma > 0$ is a constant. This auxiliary system is often called an 'observer,' since it incorporates a copy of the plant, but it is not used for state estimation in this context. The identifier also employs an additional nonlinear damping term that has the effect of dynamic normalisation.

To maintain the parabolic character, $\hat{\beta}(t) \geq \underline{\beta} > 0$, and advection direction, $\hat{\alpha}(t) \geq \underline{\alpha} > 0$, we employ projection operators. We thus choose the parameter estimate update laws as

$$\dot{\hat{\alpha}} = \rho_1 \mathrm{Proj}_{\underline{\alpha}}\left[\int_0^1 [\lambda(x,t)u_x + u](u-\hat{u})dx + \int_0^1 [-\mu(x,t)v_x + v](v-\hat{v})dx\right] \tag{40}$$

$$\dot{\hat{\beta}} = \rho_2 \mathrm{Proj}_{\underline{\beta}}\left[\int_0^1 [u_{xx}(u-\hat{u}) + v_{xx}(v-\hat{v})]\,dx\right] \tag{41}$$

which leads us to the following result.

Theorem 4.1: *The auxiliary system* (36)–(39) *with update laws* (40) *and* (41) *guarantees the following signal properties:*

$$\|\tilde{u}\|, \|\tilde{v}\|, \tilde{\alpha}, \tilde{\beta} \in \mathscr{L}_\infty \tag{42}$$

$$\tilde{u}(0), \|\tilde{u}\|, \|\tilde{u}_x\|, \tilde{v}(0), \|\tilde{v}\|, \|\tilde{v}_x\|, \|\tilde{u}\|\|u\|, \|\tilde{v}\|\|v\| \in \mathscr{L}_2 \tag{43}$$

Proof: The error signal $\tilde{u} = u - \hat{u}$, $\tilde{v} = v - \hat{v}$ satisfies the following PDE:

$$\tilde{u}_t = \hat{\alpha}\lambda(x,t)\tilde{u}_x + \hat{\beta}\tilde{u}_{xx} + \tilde{\alpha}\lambda(x,t)u_x + \tilde{\beta}u_{xx} + \tilde{\alpha}u - \gamma^2\tilde{u}\|u\|^2 \tag{44}$$

$$\tilde{v}_t = -\hat{\alpha}\mu(x,t)\tilde{v}_x + \hat{\beta}\tilde{v}_{xx} - \tilde{\alpha}\mu(x,t)v_x + \tilde{\beta}v_{xx} + \tilde{\alpha}v - \gamma^2\tilde{v}\|v\|^2 \tag{45}$$

$$\tilde{u}(1,t) = 0, \qquad \tilde{u}_x(0,t) = 0 \tag{46}$$

$$\tilde{v}(0,t) = 0, \qquad \tilde{v}_x(1,t) = 0 \tag{47}$$

Consider the Lyapunov functional as follows:

$$V(t) = \frac{1}{2}\int_0^1 \tilde{u}^2 dx + \frac{1}{2}\int_0^1 \tilde{v}^2 dx + \frac{\tilde{\alpha}^2}{2\rho_1} + \frac{\tilde{\beta}^2}{2\rho_2} \tag{48}$$

where ρ_1, $\rho_2 > 0$. The time derivative along the solution trajectories is

$$\begin{aligned}\dot{V} = &\int_0^1 [\hat{\alpha}\lambda(x,t)\tilde{u}\tilde{u}_x + \hat{\beta}\tilde{u}\tilde{u}_{xx} + \tilde{\alpha}\lambda(x,t)\tilde{u}u_x \\ &+ \tilde{\beta}\tilde{u}u_{xx} + \tilde{\alpha}\tilde{u}u - \gamma^2\tilde{u}^2\|u\|^2]dx \\ &+ \int_0^1 [-\hat{\alpha}\mu(x,t)\tilde{v}\tilde{v}_x + \hat{\beta}\tilde{v}\tilde{v}_{xx} - \tilde{\alpha}\mu(x,t)\tilde{v}v_x \\ &+ \tilde{\beta}\tilde{v}v_{xx} + \tilde{\alpha}\tilde{v}v - \gamma^2\tilde{v}^2\|v\|^2]dx - \frac{\dot{\hat{\alpha}}\tilde{\alpha}}{\rho_1} - \frac{\dot{\hat{\beta}}\tilde{\beta}}{\rho_2}\end{aligned} \tag{49}$$

Note that the first term can be written as $\hat{\alpha}\int_0^1 \lambda(x,t)\tilde{u}\tilde{u}_x dx = \frac{\hat{\alpha}}{2}\int_0^1 \lambda(x,t)\frac{\partial}{\partial x}(\tilde{u}^2)dx$. Use integration by parts and the boundary conditions (46) and (47) to obtain

$$\begin{aligned}\dot{V} = &-\frac{\hat{\alpha}}{2}\lambda(0,t)\tilde{u}^2(0) - \frac{\hat{\alpha}}{2}\lambda'\|\tilde{u}\|^2 - \hat{\beta}\|\tilde{u}_x\|^2 \\ &- \frac{\hat{\alpha}}{2}\mu(1,t)\tilde{v}^2(1) + \frac{\hat{\alpha}}{2}\mu'\|\tilde{v}\|^2 - \hat{\beta}\|\tilde{v}_x\|^2 \\ &+ \tilde{\alpha}\int_0^1 [\lambda(x,t)\tilde{u}u_x + \tilde{u}u - \mu(x,t)\tilde{v}v_x + \tilde{v}v]\,dx \\ &+ \tilde{\beta}\int_0^1 [\tilde{u}u_{xx} + \tilde{v}v_{xx}]\,dx \\ &- \gamma^2\tilde{u}^2\|u\|^2 - \gamma^2\tilde{v}^2\|v\|^2 - \frac{\dot{\hat{\alpha}}\tilde{\alpha}}{\rho_1} - \frac{\dot{\hat{\beta}}\tilde{\beta}}{\rho_2}\end{aligned} \tag{50}$$

Bounding $\hat{\alpha} \geq \underline{\alpha}$ and $\hat{\beta} \geq \underline{\beta}$, we obtain

$$\begin{aligned}\dot{V} \leq & \left[\int_0^1 [\lambda(x,t)u_x\tilde{u} + u\tilde{u} - \mu(x,t)v_x\tilde{v} + v\tilde{v}]\,dx - \frac{\dot{\hat{\alpha}}}{\rho_1}\right] \\ & \tilde{\alpha} + \left[\int_0^1 [u_{xx}\tilde{u} + v_{xx}\tilde{v}]\,dx - \frac{\dot{\hat{\beta}}}{\rho_2}\right] \\ & \tilde{\beta} - \frac{1}{2}\underline{\alpha}\lambda(0,t)\tilde{u}^2(0) - \frac{1}{2}\underline{\alpha}\lambda'\|\tilde{u}\|^2 - \underline{\beta}\|\tilde{u}_x\|^2 \\ & -\frac{1}{2}\underline{\alpha}\mu(1,t)\tilde{v}^2(1) + \frac{1}{2}\underline{\alpha}\mu'\|\tilde{v}\|^2 - \underline{\beta}\|\tilde{v}_x\|^2 \\ & -\gamma^2\|\tilde{u}\|^2\|u\|^2 - \gamma^2\|\tilde{v}\|^2\|v\|^2 \end{aligned} \tag{51}$$

Apply the update laws (40) and (41). This renders $\dot{V}$ negative semi-definite:

$$\begin{aligned}\dot{V}(t) \leq & -\frac{1}{2}\underline{\alpha}\lambda(0,t)\tilde{u}^2(0) - \frac{1}{2}\underline{\alpha}\lambda'\|\tilde{u}\|^2 - \underline{\beta}\|\tilde{u}_x\|^2 \\ & -\frac{1}{2}\underline{\alpha}\mu(1,t)\tilde{v}^2(1) + \frac{1}{2}\underline{\alpha}\mu'\|\tilde{v}\|^2 - \underline{\beta}\|\tilde{v}_x\|^2 \\ & -\gamma^2\|\tilde{u}\|^2\|u\|^2 - \gamma^2\|\tilde{v}\|^2\|v\|^2. \end{aligned} \tag{52}$$

which implies that $V(t) \leq V(0)\,\forall t \geq 0$. Using the definition of V in Equation (48), we get that $\|\tilde{u}\|$, $\|\tilde{v}\|$, $\tilde{\alpha}$, $\tilde{\beta}$ are bounded. Integrating Equation (52) with respect to time, we obtain the properties that $\tilde{u}(0)$, $\|\tilde{u}\|$, $\|\tilde{u}_x\|$, $\tilde{v}(0)$, $\|\tilde{v}\|$, $\|\tilde{v}_x\|$, $\|\tilde{u}\|\|u\|$, $\|\tilde{v}\|\|v\|$ are square integrable. This completes the proof. □

Remark 3: Hence we can claim that for any initial distributions $u(0)$ and $v(0)$, the parameter estimates and error signals will remain bounded at all times. However, due to the unstrict inequality (52), there is no guarantee that the parameter estimates will converge to the true values. Boundedness without guaranteed convergence, however, is a typical best-case theoretic result in parameter identification (for details, see Ioannou & Sun, 1996).

Remark 4: The Lyapunov analysis above enables one to show that the boundedness of the parameter estimates $\tilde{\alpha}$ and $\tilde{\beta}$ is independent of the time-varying ambient temperature $T_\infty(t)$. Namely, $T_\infty(t)$ manifests itself as the time variation in the advection speeds $\lambda(x,\ t)$ and $\mu(x,\ t)$. Majorising these terms in Equation (52) using the relations $-\lambda(0; T_\infty^{\max}) = \max_{T_\infty(t)}\{-\lambda(0,t)\}$ and $-\mu(0; T_\infty^{\min}) = \max_{T_\infty(t)}\{-\mu(1,t)\}$, we obtain

$$\begin{aligned}\dot{V}(t) \leq & -\frac{1}{2}\underline{\alpha}\lambda(0;T_\infty^{\max})\tilde{u}^2(0) - \frac{1}{2}\underline{\alpha}\lambda'\|\tilde{u}\|^2 - \underline{\beta}\|\tilde{u}_x\|^2 \\ & -\frac{1}{2}\underline{\alpha}\mu(0;T_\infty^{\min})\tilde{v}^2(1) + \frac{1}{2}\underline{\alpha}\mu'\|\tilde{v}\|^2 - \underline{\beta}\|\tilde{v}_x\|^2 \\ & -\gamma^2\|\tilde{u}\|^2\|u\|^2 - \gamma^2\|\tilde{v}\|^2\|v\|^2. \end{aligned} \tag{53}$$

Consequently, given bounded values of $T_\infty(t)$, which is always true in practice, the boundedness of the parameter estimates is independent of varying ambient temperature.

4.2 *Swapping identifier*

In this section, we consider an alternative parameter identification scheme – the swapping design. The swapping identification technique follows a common parameter identification methodology for dynamic systems. Namely, first convert a dynamic parameterisation of the plant into a static form by filtering the measured and regressor signals. Next, apply gradient or least squares estimation techniques to identify the parameters of this parametric model (Ioannou & Sun, 1996). In the derivations that follow, we follow an extension of this methodology first developed in Smyshlyaev and Krstic (2010) to boundary-coupled parabolic PDE systems, where the filters are PDEs themselves and the adaptation laws involve inner products of continuous functions instead of matrix vectors.

To this end, consider the 'estimation error' between the states u, v, and filtered signals $\sigma_1, \sigma_2, \tau_1, \tau_2, \eta_1, \eta_2, \nu_1, \nu_2$:

$$e_1 = u - \alpha\sigma_1 - \alpha\tau_1 - \beta\eta_1 - \nu_1 \tag{54}$$

$$e_2 = u - \alpha\sigma_2 - \alpha\tau_2 - \beta\eta_2 - \nu_2 \tag{55}$$

where the static parametric model is $\alpha\sigma_i + \alpha\tau_i + \beta\eta_i + \nu_i$, for $i = 1, 2$. The variables σ_i, τ_i, η_i, ν_i are outputs of Kreisselmeier filters applied to the regressor signals (see also Krstic, Kanellakopoulos, & Kokotovic, 1995). These filters are deliberately designed such that the two-state PDE system governing the estimation error, $e_1(x,\ t)$, $e_2(x,\ t)$, is exponentially stable in the $\mathscr{L}_2$-norm. In particular, we select the following PDE for (e_1, e_2):

$$e_{1t} = \hat{\alpha}\lambda(x,t)e_{1x} + \hat{\beta}e_{1xx} \tag{56}$$

$$e_{2t} = -\hat{\alpha}\mu(x,t)e_{2x} + \hat{\beta}e_{2xx} \tag{57}$$

$$e_1(1,t) = 0, \qquad e_{1x}(0,t) = 0 \tag{58}$$

$$e_2(0,t) = 0, \qquad e_{2x}(1,t) = 0 \tag{59}$$

which one can show is exponentially stable using the Lyapunov function $V(t) = 1/2\int_0^1 e_1^2(x,t)dx + 1/2\int_0^1 e_2^2(x,t)dx$. To obtain the PDEs (56)–(59) for the estimation error, the filters are designed as follows. The variables σ_1, σ_2 are the filters corresponding to u_x, v_x:

$$\sigma_{1t} = \hat{\alpha}\lambda(x,t)\sigma_{1x} + \hat{\beta}\sigma_{1xx} + \lambda(x,t)u_x \tag{60}$$

$$\sigma_{2t} = -\hat{\alpha}\mu(x,t)\sigma_{2x} + \hat{\beta}\sigma_{2xx} - \mu(x,t)v_x \tag{61}$$

$$\sigma_1(1) = 0, \qquad \sigma_{1x}(0) = 0 \tag{62}$$

$$\sigma_2(0) = 0, \qquad \sigma_{2x}(1) = 0 \tag{63}$$

The variables τ_1, τ_2 are the filters corresponding to u, v:

$$\tau_{1t} = \hat{\alpha}\lambda(x,t)\tau_{1x} + \hat{\beta}\tau_{1xx} + u \tag{64}$$

$$\tau_{2t} = -\hat{\alpha}\mu(x,t)\tau_{2x} + \hat{\beta}\tau_{2xx} + v \tag{65}$$

$$\tau_1(1) = 0, \qquad \tau_{1x}(0) = 0 \tag{66}$$

$$\tau_2(0) = 0, \qquad \tau_{2x}(1) = 0 \tag{67}$$

The variables η_1, η_2 are the filters corresponding to u_{xx}, v_{xx}:

$$\eta_{1t} = \hat{\alpha}\lambda(x,t)\eta_{1x} + \hat{\beta}\eta_{1xx} + u_{xx} \tag{68}$$

$$\eta_{2t} = -\hat{\alpha}\mu(x,t)\eta_{2x} + \hat{\beta}\eta_{2xx} + v_{xx} \tag{69}$$

$$\eta_1(1) = 0, \qquad \eta_{1x}(0) = 0 \tag{70}$$

$$\eta_2(0) = 0, \qquad \eta_{2x}(1) = 0 \tag{71}$$

The variables ν_1, ν_2 are the following filters:

$$\nu_{1t} = \hat{\alpha}\lambda(x,t)\nu_{1x} + \hat{\beta}\nu_{1xx} - \hat{\alpha}\lambda(x,t)u_x - \hat{\beta}u_{xx} \tag{72}$$

$$\nu_{2t} = -\hat{\alpha}\mu(x,t)\nu_{2x} + \hat{\beta}\nu_{2xx} + \hat{\alpha}\mu(x,t)v_x - \hat{\beta}v_{xx} \tag{73}$$

$$\nu_1(1) = q_1(t)v(1), \qquad \nu_{1x}(0) = -v_x(0) \tag{74}$$

$$\nu_2(0) = q_2(t)u(0), \qquad \nu_{2x}(1) = -u_x(1) \tag{75}$$

We now form the 'parameter prediction error' as

$$\hat{e}_1 = u - \hat{\alpha}\sigma_1 - \hat{\alpha}\tau_1 - \hat{\beta}\eta_1 - \nu_1 \tag{76}$$

$$\hat{e}_2 = v - \hat{\alpha}\sigma_2 - \hat{\alpha}\tau_2 - \hat{\beta}\eta_2 - \nu_2 \tag{77}$$

Using this parametric model, we implement the following gradient update laws:

$$\dot{\hat{\alpha}} = \rho_\alpha \mathrm{Proj}_{\underline{\alpha}} \int_0^1 [\hat{e}_1(\sigma_1 + \tau_1) + \hat{e}_2(\sigma_2 + \tau_2)]\,dx \tag{78}$$

$$\dot{\hat{\beta}} = \rho_\beta \mathrm{Proj}_{\underline{\beta}} \int_0^1 [\hat{e}_1\eta_1 + \hat{e}_2\eta_2]\,dx \tag{79}$$

with ρ_α, $\rho_\beta > 0$. In Equation (78), we use the projection operator to conserve the direction of advection, namely, $\hat{\alpha} \geq \underline{\alpha} > 0$. In Equation (79), projection conserves the parabolic character of the system, namely, $\hat{\beta} \geq \underline{\beta} > 0$. Consequently, we arrive at a swapping identifier design with the signal properties summarised by the following theorem.

Theorem 4.2: *The filters* (60)–(75) *with parameter prediction errors* (76) *and* (77) *and update laws* (78) *and* (79) *guarantee the following signal properties:*

$$\tilde{\alpha}, \quad \tilde{\beta} \in \mathscr{L}_\infty \tag{80}$$

$$\|\hat{e}_1\|, \|\hat{e}_2\| \in \mathscr{L}_2 \cap \mathscr{L}_\infty \tag{81}$$

$$\dot{\hat{\alpha}}, \quad \dot{\hat{\beta}} \in \mathscr{L}_2 \cap \mathscr{L}_\infty \tag{82}$$

Proof: Consider the following Lyapunov function as follows:

$$V(t) = \frac{1}{2}\int_0^1 e_1^2 dx + \frac{1}{2}\int_0^1 e_2^2 dx + \frac{c}{2\rho_\alpha}\tilde{\alpha}^2 + \frac{c}{2\rho_\beta}\tilde{\beta}^2 \tag{83}$$

where $c = \max\{\lambda'\underline{\alpha}, -\mu'\underline{\alpha}\} > 0$. The time derivative along the solution trajectories is

$$\begin{aligned}\dot{V}(t) = &\int_0^1 \hat{\alpha}\lambda(x,t)e_1e_{1x}dx + \int_0^1 \hat{\beta}e_1e_{1xx}dx \\ &- \int_0^1 \hat{\alpha}\mu(x,t)e_2e_{2x}dx + \int_0^1 \hat{\beta}e_2e_{2xx}dx \\ &- \frac{c}{\rho_\alpha}\tilde{\alpha}\dot{\hat{\alpha}} - \frac{c}{\rho_\beta}\tilde{\beta}\dot{\hat{\beta}}\end{aligned} \tag{84}$$

Note that the first term can be written as $\hat{\alpha}\int_0^1 \lambda(x,t)e_1e_{1x}dx = \frac{\hat{\alpha}}{2}\int_0^1 \lambda(x,t)\frac{\partial}{\partial x}(e_1^2)dx$, and similarly for the third term. Use integration by parts, boundary conditions (58) and (59), and update laws (78) and (79) to obtain

$$\begin{aligned}\dot{V}(t) = &-\frac{\hat{\alpha}}{2}\lambda(0,t)e_1^2(0) - \frac{\hat{\alpha}}{2}\lambda'\|e_1\|^2 - \hat{\beta}\|e_{1x}\|^2 \\ &- \frac{\hat{\alpha}}{2}\mu(1,t)e_2^2(1) + \frac{\hat{\alpha}}{2}\mu'\|e_2\|^2 - \hat{\beta}\|e_{2x}\|^2 \\ &- c\int_0^1 \hat{e}_1\left[\tilde{\alpha}(\sigma_1 + \tau_1) + \tilde{\beta}\eta_1\right]dx \\ &- c\int_0^1 \hat{e}_2\left[\tilde{\alpha}(\sigma_2 + \tau_2) + \tilde{\beta}\eta_2\right]dx\end{aligned} \tag{85}$$

Note that $\hat{e}_i - e_i = \tilde{\alpha}(\sigma_i + \tau_i) + \tilde{\beta}\eta_i$, for $i = 1, 2$. We now have

$$\begin{aligned}\dot{V}(t) = &-\frac{\hat{\alpha}}{2}\lambda(0,t)e_1^2(0) - \frac{\hat{\alpha}}{2}\lambda'\|e_1\|^2 - \hat{\beta}\|e_{1x}\|^2 \\ &- \frac{\hat{\alpha}}{2}\mu(1,t)e_2^2(1) + \frac{\hat{\alpha}}{2}\mu'\|e_2\|^2 - \hat{\beta}\|e_{2x}\|^2 \\ &- c\|\hat{e}_1\|^2 + c\int_0^1 \hat{e}_1e_1dx - c\|\hat{e}_2\|^2 + c\int_0^1 \hat{e}_2e_2dx\end{aligned} \tag{86}$$

Now use the Cauchy–Schwarz and Young's inequality as follows:

$$c\int_0^1 \hat{e}_i e_i dx \le c\|\hat{e}_i\|\cdot\|e_1\| \le \frac{c}{2}\|\hat{e}_i\|^2 + \frac{c}{2}\|e_i\|^2, \quad \text{for} \quad i=1,2 \tag{87}$$

which renders the following upper bound estimate on $\dot{V}$

$$\begin{aligned}\dot{V}(t) \le & -\frac{\hat{\alpha}}{2}\lambda(0,t)e_1^2(0) - \hat{\beta}\|e_{1x}\|^2 + \frac{1}{2}[c-\hat{\alpha}\lambda']\|e_1\|^2 \\ & -\frac{\hat{\alpha}}{2}\mu(1,t)e_2^2(1) - \hat{\beta}\|e_{2x}\|^2 + \frac{1}{2}[c+\hat{\alpha}\mu']\|e_2\|^2 \\ & -\frac{c}{2}\|\hat{e}_1\|^2 - \frac{c}{2}\|\hat{e}_2\|^2\end{aligned} \tag{88}$$

Using the definition $c = \max\{\lambda'\underline{\alpha}, -\mu'\underline{\alpha}\}$ and lower bounds on α and β, we arrive at the final upper bound estimate of $\dot{V}$:

$$\begin{aligned}\dot{V}(t) \le & -\frac{\underline{\alpha}}{2}\lambda(0,t)e_1^2(0) - \underline{\beta}\|e_{1x}\|^2 - \frac{\underline{\alpha}}{2}\mu(1,t)e_2^2(1) \\ & -\underline{\beta}\|e_{2x}\|^2 - \frac{c}{2}\|\hat{e}_1\|^2 - \frac{c}{2}\|\hat{e}_2\|^2 \le 0\end{aligned} \tag{89}$$

which implies that $V(t) \le V(0)$, and from the definition of V in Equation (83), we get that $\|e_1\|, \|e_2\|, \tilde{\alpha}, \tilde{\beta}$ are bounded. Integrating Equation (89) with respect to time from zero to infinity, we get the properties $\|\hat{e}_1\|, \|\hat{e}_2\| \in \mathscr{L}_2 \cap \mathscr{L}_\infty$. From the update laws (78) and (79), we conclude that $\dot{\hat{\alpha}}, \dot{\hat{\beta}} \in \mathscr{L}_2 \cap \mathscr{L}_\infty$, which provides all the signal properties in Equations (80)–(82).

Remark 5: Similar to Remark 4, the Lyapunov analysis above enables one to show that the boundedness of the parameter estimates $\tilde{\alpha}$ and $\tilde{\beta}$ is independent of the time-varying ambient temperature $T_\infty(t)$. Majorising the advection speed terms with respect to T_∞ in Equation (89) as before, we obtain

$$\begin{aligned}\dot{V}(t) \le & -\frac{\underline{\alpha}}{2}\lambda(0;T_\infty^{\max})e_1^2(0) - \underline{\beta}\|e_{1x}\|^2 - \frac{\underline{\alpha}}{2}\mu(0;T_\infty^{\min})e_2^2(1) \\ & -\underline{\beta}\|e_{2x}\|^2 - \frac{c}{2}\|\hat{e}_1\|^2 - \frac{c}{2}\|\hat{e}_2\|^2 \le 0\end{aligned} \tag{90}$$

Consequently, given bounded values of $T_\infty(t)$, which is always true in practice, the boundedness of the parameter estimates is independent of varying ambient temperature.

5. Simulations and discussion

Next, we study the behaviour of the passive and swapping identification algorithms by examining four scenarios. Namely, the identifiers are provided plant data from (Case A) the PDE model (20)–(25), (Case B) the PDE model (20)–(25) with noise, (Case C) 1000 individual TCLs, and (Case D) 1000 stochastic TCLs with disturbance $w(t)$ distributed with standard deviation $\sigma_w = 0.01$ (Callaway, 2009; Perfumo et al., 2012). In all cases, the identifiers are incorrectly initialised with parameter estimates $\hat{\alpha}(0) = 0.1\alpha$ and $\hat{\beta}(0) = 10\beta$. To assess model fit, we also plot the identifier error as a function of time, given by $\|\tilde{u}\| + \|\tilde{v}\|$ for the passive identifier and $\|\hat{e}_1\| + \|\hat{e}_2\|$ for the swapping identifier. The following lower bounds are also used: $\underline{\alpha} = 0.01$, $\underline{\beta} = 0.005$. Each algorithm is implemented using the Crank–Nicolson finite-differencing method (Crank & Nicolson, 1947).

5.1 *Passive identifier*

First, we consider the passive identification scheme from Section 4.1, with parameters $\rho_1 = 10^{-3}$, $\rho_2 = 10^{-3}$, $\gamma = 1$, and $\hat{u}(x,0) = u(x,0)$, $\hat{v}(x,0) = v(x,0)$. Figure 6 demonstrates how the parameter estimates evolve under Case A. Subplots (a) and (b) demonstrate the evolution of the parameter estimates $\hat{\alpha}$ and $\hat{\beta}$, respectively. Indeed, the estimation errors are bounded according to Theorem 4.1 and, in addition, converge near their true values. Subplot (c) demonstrates how the $\mathscr{L}_2$ norms of the identifier's error states are also bounded and decay towards zero over time. Thus, the identifier performs as expected in the ideal case.

For Case B, we add Gaussian noise with zero mean and a standard deviation equal to $0.01\max_{x\in[0,1]}u(0)$ to $u(x,t)$ and $v(x,t)$ throughout the interval $x \in [0,1]$. The simulation parameters are otherwise identical to the first case. The parameter estimates are shown in Figure 6(a). In this case,

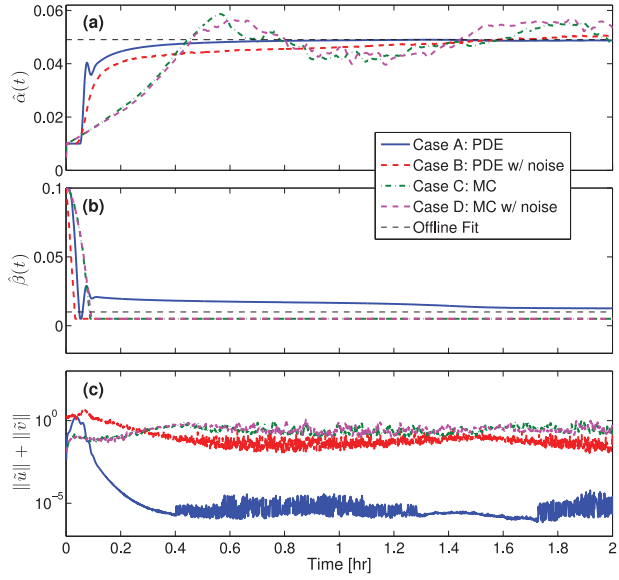

Figure 6. Simulations of the passive identifier under Case A, using auxiliary system (36)–(39) and update laws (40) and (41). Subplots (a) and (b) demonstrate the evolution of the parameter estimates $\hat{\alpha}$ and $\hat{\beta}$, respectively. Subplot (c) demonstrates the model fit in terms of how the $\mathscr{L}_2$ norm of the identifier's error states decay over time.

we see that $\hat{\alpha}$ converges to the vicinity of the true value of α at almost the same rate as above, whereas $\hat{\beta}$ decreases toward zero. Once it reaches the projection boundary, it stays at that value. In this case, the measurements do not have a sufficiently high signal-to-noise ratio to differentiate between noise and the second spatial derivative.

In Case C, we identify the parameters $\hat{\alpha}$ and $\hat{\beta}$ based on data obtained from an MC simulation of 1000 TCLs. This can be considered a proxy for a smart grid scenario, where the TCLs are able to communicate their temperature states to a central server and (u, v) are computed directly from that data. The TCL parameters are given in Table 1. The temperature interval is divided into 20 equal intervals, and the number of TCLs whose temperatures fall within each sub-interval is counted as the value of u or v at that temperature. The data are smoothed using an averaging filter along the temperature interval. The passive parameter identification is then executed on the smoothed data. The results of the passive identifier are shown in Figure 6. As before, the parameters converge within a neighbourhood of the offline fitted values. However, the region of convergence is larger due to the error induced by using a PDE model of the population. Nevertheless, the identifier error, shown in Figure 6(c), is nearly the same order as the PDE model with measurement noise. Case D considers a *stochastic* population of TCLs, and the results are shown in Figure 6. In this case, the convergence results and identifier error is similar to Case C.

5.2 *Swapping identifier*

Next, we consider the swapping identification scheme from Section 4.2, with parameters $\rho_\alpha = \rho_\beta = 20$. All filters are initialised at zero, except $v_1(x, 0) = u(x, 0)$ and $v_2(x, 0) = v(x, t)$. Figure 7 demonstrates how the parameter estimates evolve under Case A. Subplots (a) and (b) demonstrate the evolution of the parameter estimates $\hat{\alpha}$ and $\hat{\beta}$, respectively. Indeed, the estimation errors are bounded according to Theorem 4.2 and, in addition, converge near their true values. Subplot (c) demonstrates how the $\mathscr{L}_2$ norms of the parametric error $(\hat{e}_1, \hat{e}_2)$ are also bounded and decay towards zero over time. Thus, the identifier performs as expected in the ideal case.

For Case B, we add Gaussian noise as before. The simulation parameters are otherwise identical to the first case. The parameter estimates are shown in Figure 7(a). In this case, we see that the convergence of $\hat{\alpha}$ and $\hat{\beta}$ is almost indiscernible from Case A, since the filters successfully attenuate the measurement noise. The identifier model error, however, reaches a larger steady-state error than the noise-free case.

Next, we consider Case C where the individual TCL data is smoothed using an averaging filter along the temperature interval. The result of the parameter fitting is shown in Figure 7. The estimate $\hat{\alpha}$ converges within a smaller neighbourhood of its true value, as compared to the passive identifier. Indeed, the filters provide the added role of removing noise, and therefore, the swapping identification scheme provides more accurate estimates than the passive scheme. Nevertheless, the estimate for $\hat{\beta}$ decreases toward zero and remains at the projection boundary, due to a lack of persistent excitation. Case D, which considers a stochastic TCL population, exhibits very similar results to Case C. As before, the filters inherently remove the noise and identify the parameters by capturing the inherent diffusion–advection dynamics of the population.

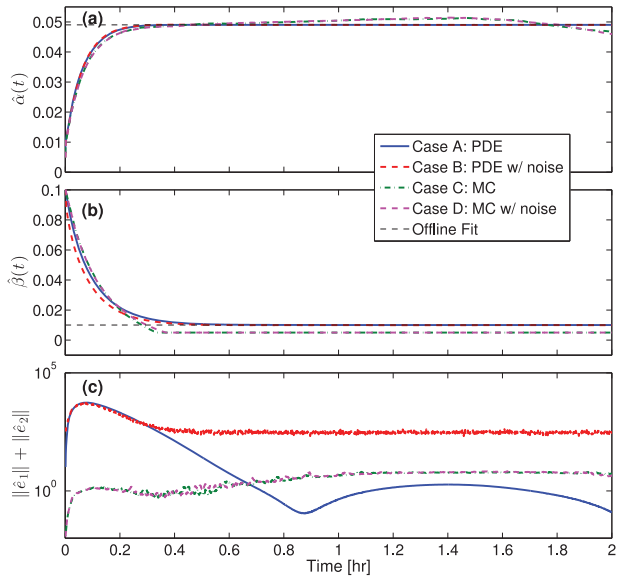

Figure 7. Simulations of the swapping identifier under *Case A*, using filters (60)–(75) with parameter prediction errors (76) and (77) and update laws (78) and (79). Subplots (a) and (b) demonstrate the evolution of the parameter estimates $\hat{\alpha}$ and $\hat{\beta}$, respectively. Subplot (c) demonstrates the model fit in terms of how the $\mathscr{L}_2$ norm of the error states $(\hat{e}_1, \hat{e}_2)$ decay over time.

5.3 *A controlled TCL population*

In this section, we consider each identification algorithm under a control input scenario in Case D. That is, we apply the identification algorithms to a stochastic population of TCLs undergoing a forced input that changes the aggregate power consumption. In particular, we consider the forced switching control proposed by Mathieu et al. (2013). In this control framework, we consider a control parameter σ, which represents the fraction of TCLs in the population we force to switch *off* instantaneously at time $t = t_0$. The TCLs that switch are random, and can be mathematically actuated by considering a random variable generated from the uniform distribution, $m_i \sim \mathscr{U}(0, 1)$, and the switching condition $m_i < \sigma$, for each TCL, $i = 1, 2, \ldots, N$. Consequently, the controlled switching is modified from Equation (2)

Table 3. Comparison of passive and swapping identification methods.

Property	Passive identifier	Swapping identifier
Dynamic order	One two-state PDE for the auxiliary system	Four two-state PDEs for the filters
Nonlinear complexity	The auxiliary system and update law are nonlinear	The filters are linear, but the update law is generally nonlinear
Sensitivity to noise/ model uncertainty	No attenuation of noise induced from $(\cdot)_x$, $(\cdot)_{xx}$ measurements	Filters attenuate noise induced from $(\cdot)_x$, $(\cdot)_{xx}$ measurements

to be

$$s_i(t_0) = \begin{cases} 0 & \text{if } s_i(t_0-\varepsilon)=1 \text{ and } T_i(t) \le T_{\min,i} \\ 1 & \text{if } s_i(t_0-\varepsilon)=0 \text{ and } T_i(t) \ge T_{\max,i} \\ 0 & \text{if } m_i < \sigma \\ s_i(t_0-\varepsilon) & \text{otherwise} \end{cases} \tag{91}$$

Figure 8 demonstrates how each algorithm performs under a forced switching scenario. In this example, $\sigma = 0.5$, meaning 50% of the TCLs switch off at time $t = 2$ hr, as can be seen in Figure 8(c). Note that this forced switching creates a disturbance in the parameter estimates. However, the estimates stay bounded within a neighbourhood of their offline fitted values. As a result, the parameter identification algorithms are applicable to a non-autonomous population of TCLs for demand side management.

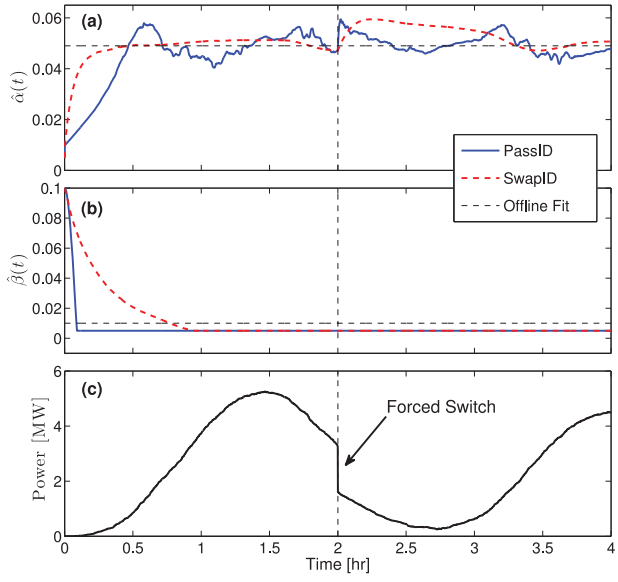

Figure 8. Simulations of the passive and swapping identifier under *Case D* with 50% of the TCLs forced to switch *off* at time $t = 2$ hr. Subplots (a) and (b) demonstrate the evolution of the parameter estimates $\hat{\alpha}$ and $\hat{\beta}$, respectively. Subplot (c) demonstrates the aggregate power of the stochastic TCL population, with 50% of the TCLs switched off at time $t = 2$ hr.

5.4 *Comparative analysis*

In this paper, we have derived, implemented, and analysed two different parameter identification schemes for PDE models of heterogeneous TCL populations. Next, we examine the relative strengths and weaknesses of each identification algorithm, summarised in Table 3.

From an implementation perspective, the passive identification algorithm has a smaller dynamic order (one PDE versus four PDEs). However, the auxiliary system is nonlinear, whereas the filters in the swapping identifier are linear. From a robustness perspective, the swapping identifier exhibits more accurate estimates in the presence of noise. In particular, the filters attenuate measurement noise resulting in improved estimates for the first and second spatial derivatives of the PDEs. More importantly, the swapping identifier demonstrates robustness to modelling errors, as demonstrated by the results on deterministic and stochastic TCL populations.

6. Conclusion

This paper develops methods for model identification of aggregated TCLs in a smart grid setting using PDE techniques. First, a two-state boundary-coupled hyperbolic PDE model for homogenous TCL populations was derived based on a hybrid ODE model of a single TCL. An important feature of the population behaviour is that, under parameter homogeneity, the aggregated power consumption exhibits undamped oscillations. In the case of heterogeneous TCL populations, the power consumption exhibits damped oscillations due to a diffusive effect on the TCL density dynamics. Consequently, this paper proposes to add a diffusive term to the boundary-coupled PDEs to model heterogeneous TCL populations.

Next, two parameter identification schemes are derived for the heterogeneous PDE models: a passive and a swapping scheme. We prove signal properties for each identifier, in terms of relevant error norms. Although there is no guarantee that the parameters will converge to the true values, simulations indicate that parameter estimates converge within a neighbourhood of the true values in the absence of noise. In the presence of noise, the swapping identifier generally exhibits improved convergence accuracy over the passive identifier, at the cost of implementation complexity.

For MC simulations of deterministic and stochastic TCLs, the converged parameter estimates are consistent with the offline model fit performed in Section 3.3. Moreover, the algorithms are applicable to a controlled population of TCLs.

Future work focuses on robust model identification techniques, incorporating these estimates into adaptive control of TCL populations, and application to TCLs on a university campus.

Acknowledgements

The first author wishes to acknowledge the assistance of Paul-Hervé Tamokoue Kamga during his internship at University of California Berkeley. The second author is grateful for the support granted by the Otto Mønsted and Dir. Ib Henriksen foundations.

References

Andersen, P., Pedersen, T.S., & Nielsen, K.M. (2012, October). *Observer based model identification of heat pumps in a smart grid*. Proceedings of Multiconference on Systems and Control, Dubrovnik. doi:10.1109/CCA.2012.6402428.

Banakar, H., Luo, C., & Ooi, B.T. (2008). Impacts of wind power minute-to-minute variations on power system operation. *IEEE Transactions on Power Systems, 23*, 150–160.

Bashash, S., & Fathy, H. (2013). Modeling and control of aggregate air conditioning loads for robust renewable power management. *IEEE Transactions on Control Systems Technology, 21*, 1318–1327.

Bompard, E., Carpaneto, E., Chicco, G., & Napoli, R. (1996). Analysis and modelling of thermostatically-controlled loads. In *Proceedings of 8th Mediterranean Electrotechnical Conference* (Vol. 2, pp. 730–734). Bari: IEEE.

Callaway, D. (2009). Tapping the energy storage potential in electric loads to deliver load following and regulation, with application to wind energy. *Energy Conversion and Management, 50*, 1389–1400.

Callaway, D., & Hiskens, I. (2011). Achieving controllability of electric loads. *Proceedings of the IEEE, 99*, 184–199.

Crank, J., & Nicolson, P. (1947). A practical method for numerical evaluation of solutions of partial differential equations of the heat conduction type. *Proceedings of the Cambridge Philosophical Society, 43*, 50–67.

International Energy Agency. (2006). *World energy outlook 2006* (Technical report). Paris: Organisation for Economic Co-operation and Development.

Ioannou, P., & Sun, J. (1996). *Robust adaptive control*. Upper Saddle River, NJ: Prentice-Hall.

Klobasa, M. (2010). Analysis of demand response and wind integration in Germany's electricity market. *IET Renewable Power Generation, 4*, 55–63.

Krstic, M., Kanellakopoulos, I., & Kokotovic, P. (1995). *Nonlinear and adaptive control design*. New York, NY: Wiley.

Kundu, S., & Sinitsyn, N. (2012, June). *Safe protocol for controlling power consumption by a heterogeneous population of loads*. Proceedings of 2012 American Control Conference, Montreal, QC.

Lu, N., Chassin, D.P., & Widergren, S.E. (2005). Modeling uncertainties in aggregated thermostatically controlled loads using a state queueing model. *IEEE Transactions on Power Systems, 20*, 725–733.

MacCormack, R.W. (2003). The effect of viscosity in hypervelocity impact cratering. *Journal of Spacecraft and Rockets, 40*, 757–763.

Malhame, R., & Chong, C. (1985). Electric load model synthesis by diffusion approximation of a higher-order hybrid-state stochastic system. *IEEE Transactions on Automatic Control, 30*, 854–860.

Mathieu, J.L., Koch, S., & Callaway, D.S. (2013). State estimation and control of electric loads to manage real-time energy imbalance. *IEEE Transactions on Power Systems, 28*, 430–440.

McDonald, H. (2008). Adaptive intelligent power systems: Active distribution networks. *Energy Policy, 36*, 4346–4351. doi:10.1016/j.enpol.2008.09.038.

Mets, K., Verschueren, T., Haerick, W., Develder, C., & Turck, F.D. (2010). Optimizing smart energy control strategies for plug-in hybrid electric vehicle charging. In *Network Operations and Management Symposium Workshops* (pp. 293–299). Osaka: IEEE. doi:10.1109/NOMSW.2010.5486561.

Mohsenian-Rad, A., Wong, V.W.S., Jatskevich, J., Schober, R., & Leon-Garcia, A. (2010). Autonomous demand-side management based on game-theoretic energy consumption scheduling for the future smart grid. *IEEE Transactions on Smart Grid, 1*, 320–331.

Moslehi, K., & Kumar, R. (2010). A reliability perspective of the smart grid. *IEEE Transactions on Smart Grid, 1*, 57–64.

Moura, S.J., Ruiz, V., & Bendsten, J. (2013, December). *Observer design for boundary coupled PDEs: Application to thermostatically controlled loads in smart grids*. 52nd IEEE Conference on Decision and Control, Florence.

Perfumo, C., Kofman, E., Braslavsky, J., & Ward, J. (2012). Load management: Model-based control of aggregate power for populations of thermostatically controlled loads. *Energy Conversion and Management, 55*, 36–48.

Petersen, M., Bendtsen, J., & Stoustrup, J. (2012, June). *Optimal dispatch strategy for the agile virtual power plant imbalance compensation problem*. Proceedings of American Control Conference, Montreal.

Short, J., Infield, D.G., & Freris, L.L. (2007). Stabilization of grid frequency through dynamic demand control. *IEEE Transactions on Power Systems, 22*, 1284–1293.

Smyshlyaev, A., & Krstic, M. (2010). *Adaptive control of parabolic PDEs*. Philadelphia, PA: Princeton University Press.

Strbac, G. (2008). Demand side management: Benefits and challenges. *Energy Policy, 36*, 4419–4426.

Walawalkar, R., Blumsack, S., Apt, J., & Fernands, S. (2008). An economic welfare analysis of demand response in the PJM electricity market. *Energy Policy, 36*, 3692–3702.

Zhang, W., Lian, J., Chang, C.Y., Kalsi, K., & Sun, Y. (2012, December). *Reduced-order modeling of aggregated thermostatic loads with demand response*. Proceedings of 51st IEEE Conference on Decision and Control, Maui, HI.